THE JOURNAL OF BIOLOGICAL CHEMISTRY VOL. 286, NO. 26, pp. 23441–23451, July 1, 2011

ATP and Mg^{2+} Promote the Reversible Oligomerization and Aggregation of Chloroplast 2-Cys Peroxiredoxin*[S]

Received for publication, March 14, 2011, and in revised form, April 17, 2011 Published, JBC Papers in Press, April 27, 2011, DOI 10.1074/jbc.M111.239434

Martín Aran[‡1], Diego Ferrero[‡2], Alejandro Wolosiuk[§1,3], Santiago Mora-García[‡1], and Ricardo A. Wolosiuk[‡1,4]

From the [‡]Instituto Leloir, Instituto de Investigaciones Bioquímicas-Buenos Aires, Consejo Nacional de Investigaciones Científicas y Técnicas, Depto. Química Biológica-Facultad de Ciencias Exactas y Naturales, Universidad de Buenos Aires, Patricias Argentinas 435, C1405BWE Buenos Aires, Argentina and [§]Gerencia Química, Comisión Nacional de Energía Atómica, Avda. Gral. Paz 1499, B1650KNA San Martín, Argentina

2-Cys peroxiredoxins (2-Cys Prxs) are ubiquitous peroxidases with important roles in cellular antioxidant defense and hydrogen peroxide-mediated signaling. Post-translational modifications of conserved cysteines cause the transition from low to high molecular weight oligomers, triggering the functional change from peroxidase to molecular chaperone. However, it remains unclear how non-covalent interactions of 2-Cys Prx with metabolites modulate the quaternary structure. Here, we disclose that ATP and Mg^{2+} (ATP/Mg) promote the self-polymerization of chloroplast 2-Cys Prx (polypeptide 23.5 kDa) into soluble higher order assemblies (>2 MDa) that proceed to insoluble aggregates beyond 5 mM ATP. Remarkably, the withdrawal of ATP or Mg^{2+} brings soluble oligomers and insoluble aggregates back to the native conformation without compromising the associated functions. As confirmed by transmission electron microscopy, ATP/Mg drive the toroid-like decamers (diameter 13 nm) to the formation of large sphere-like particles (diameter ~30 nm). Circular dichroism studies on ATP-labeled 2-Cys Prx reveal that ATP/Mg enhance the proportion of β-sheets with the concurrent decrease in the content of α-helices. In line with this observation, the formation of insoluble aggregates is strongly prevented by 2,2,2-trifluoroethanol, a cosolvent employed to induce α-helical conformations. We further find that the response of self-polymerization to ATP/Mg departs abruptly from that of the associated peroxidase and chaperone activities when two highly conserved residues, Arg^{129} and Arg^{152}, are mutated. Collectively, our data uncover that non-covalent interactions of ATP/Mg with 2-Cys Prx modulate dynamically the quaternary structure, thereby coupling the non-redox chemistry of cell energy with redox transformations at cysteine residues.

Peroxiredoxins (Prxs)[5] have received considerable attention as ubiquitous peroxidases with important roles in the detoxification of peroxides and H_2O_2-mediated signaling cascades (1). In the catalytic cycle, a highly conserved cysteine, named peroxidatic cysteine (Cys_P), is readily oxidized to sulfenic acid (Prx-(Cys_P)-SH + RO-OH ⇒ Prx-(Cys_P)-SOH + ROH). Next, two successive reactions bring the oxyacid of organic sulfur back to the thiol form: (i) the sulfenic acid reacts with a thiol group, forming a disulfide bond (Prx-(Cys_P)-SOH + HS-X ⇒ Prx-(Cys_P)-S-S-X + H_2O), and (ii) a thiol-disulfide exchange with protein-disulfide oxidoreductases (*e.g.* thioredoxin (Trx)) closes the peroxidatic cycle (Prx-(Cys_P)-S-S-X + $(HS)_2$-Trx ⇒ Prx-(Cys_P)-SH + HS-X + $(S)_2$-Trx) (2). With the rapid increase in structural and functional information, Prxs were assigned to various subfamilies (3–6). The widespread subfamily of typical 2-Cys Prxs features an additional cysteine residue at the C-terminal region, called resolving cysteine (Cys_R), whose thiol group reacts with the sulfenic acid of Cys_P, forming an intermolecular disulfide bond in the peroxidatic cycle (2-CysPrx-(Cys_P)-SOH + HS-(Cys_R)-2-CysPrx ⇒ 2-CysPrx-(Cys_P)-S-S-(Cys_R)-2-CysPrx + H_2O). Peroxides further oxidize Cys_P to sulfinic acid (Prx-(Cys_P)-SO_2H) in the enzymatic cycling, halting the peroxidase capacity and concurrently promoting an ATP-independent chaperone activity (7–10). The inactivation through the overoxidation of -Cys_P may play a role as a "floodgate" that restricts the scavenging of peroxides at high levels of H_2O_2 and allows signaling cross-talk with other pathways (1).

2-Cys Prxs have the ability to alternate between different levels of oligomerization, depending on the redox status of cysteine residues, pH, and the concentrations of the protein and solutes (2). In the oxidized state and low protein concentrations, 2-Cys Prxs are mainly found as covalently linked homodimers (α_2). At higher concentrations or when the cysteines are reduced or overoxidized, dimers associate into doughnut-shaped decamers $(\alpha_2)_5$ (11, 12), which, in turn, may proceed to higher order assemblies, like dodecahedrons, $((\alpha_2)_5)_{12}$ (13). By multimerization, 2-Cys Prx acquires a chaperone activity that prevents protein aggregation induced by heat shock, thereby revealing the ability to heterologously interact with other structures. Consistent with the latter capacity, 2-Cys Prxs associate with erythrocyte and chloroplast membranes in response to a broad range of stresses (14–17) and also interact

* This study was supported by grants from the Agencia Nacional de Promoción Científica y Tecnológica (ANPCyT) and Universidad de Buenos Aires.
[S] The on-line version of this article (available at http://www.jbc.org) contains supplemental Table S1 and Figs. S1–S4.
[1] Established Investigator of Consejo Nacional de Investigaciones Científicas y Técnicas (CONICET).
[2] Present address: Centro Nacional de Biotecnología, 28049 Madrid, España.
[3] Member of Centro Interdisciplinario de Nanociencia y Nanotecnología-CONICET.
[4] To whom correspondence should be addressed: Instituto Leloir, Patricias Argentinas 435, C1405BWE Buenos Aires, Argentina. Tel.: 54-11-5238-7500; Fax: 54-11-5238-7501; E-mail: rwolosiuk@leloir.org.ar.
[5] The abbreviations used are: Prx, peroxiredoxin; Cys_P, peroxidatic cysteine; Cys_R, resolving cysteine; ANS, 8-anilino-1-naphthalene-sulfonic acid; D_H, hydrodynamic diameter; DLS, dynamic light scattering; SLS, static light scattering; SPR, surface plasmon resonance; TEM, transmission electron microscopy; Trx, thioredoxin; TFE, 2,2,2-trifluoroethanol; ATP/Mg, ATP and Mg^{2+}.

non-covalently with chloroplast components, such as fructose-1,6-bisphosphatase (18), NADPH-dependent thioredoxin reductase C, cyclophilin 20-3, and photosystem II (19).

Given their link with oxidative stress, most studies on 2-Cys Prxs have examined the H_2O_2-scavenging activity and the availability of electron donors (2). Even after the thermodynamic requirements for the removal of H_2O_2 are factored in, however, cellular components unable to transfer electrons may convey a kinetic advantage due to the allosteric control of catalytic activity. In this aspect, a plethora of studies have analyzed the redox control of non-redox reactions (20–22), but detailed research on the regulation of redox processes via non-covalent interactions has proved elusive, perhaps simply because most of the conceptualizations on oxidative stress are built around redox transformations. We recently reported that ATP and Mg^{2+} (referred to hereafter as ATP/Mg) act both as substrate for autophosphorylation of the resolving cysteine Cys_R and as inhibitor of the peroxidase activity of chloroplast 2-Cys Prx (7). This dual capacity of ATP/Mg certainly warrants further examination because the nucleotide may convey the information needed for the response of 2-Cys Prx to non-redox stimuli. We found that low concentrations of ATP strongly favor the conversion of oxidized decamers into large soluble oligomers, which proceed to amorphous precipitates at higher concentrations of the nucleotide (≥5 mM). In this context, the term "oligomerization" refers to different non-covalent associations wherein 2-Cys Prx remains operationally soluble, whereas "aggregation" applies to the formation of precipitates. Significantly, both soluble oligomers and insoluble aggregates can be brought back to decamers by lowering the concentration of ATP or chelating Mg^{2+}. We further demonstrate that (i) ATP/Mg predispose oxidized 2-Cys Prx to self-polymerization by increasing the abundance of β-structures and concurrently lowering the content of α-helices, and (ii) the substitution of essential residues for peroxidase activity promotes different responses in the ability to aggregate and to act as a chaperone. These findings reveal that ATP and Mg^{2+}, two components devoid of redox activity and located in multiple cellular compartments, can modulate reversibly the assembly of 2-Cys Prx (decamers ⇔ soluble oligomers ⇔ insoluble aggregates). Hence, switching between different quaternary structures may be viewed as a mechanism that links the non-redox chemistry of the cell to the archetypical redox signaling module that is regulated through cysteine modifications.

EXPERIMENTAL PROCEDURES

Materials—Biochemicals were purchased from Sigma-Aldrich.

Construction of 2-Cys Prx Mutants—The pET-22b(+) vector (Novagen, Madison, WI) was used to express the variants of 2-Cys Prx as C-terminal hexahistidine-tagged fusion proteins in JM109 (DE3) *Escherichia coli* cells. Site-directed mutagenesis was carried out by the megaprimer method with primers described in supplemental Table S1.

Protein Purification—Recombinant chloroplast rapeseed 2-Cys Prx was prepared as described previously (18). Briefly, JM109 (DE3) *E. coli* cells harboring 2-Cys Prx expression plasmids were grown at 37 °C in Luria-Bertani medium supplemented with 100 μg/ml ampicillin. After induction with 0.6 mM isopropyl β-D-thiogalactoside, bacteria were harvested by centrifugation (3,000 × *g*, 10 min), washed with 20 mM Tris-HCl buffer (pH 8.0), resuspended in the same buffer containing 0.5 M NaCl, and subjected to sonication. After centrifugation (20,000 × *g*, 30 min), the supernatant fraction was loaded on a Ni^{2+}-iminodiacetate-Sepharose column that was washed with 20 mM Tris-HCl buffer (pH 8.0) containing successively 60 and 600 mM imidazole. The protein fraction released in the latter elution was dialyzed against and stored in 20 mM Tris-HCl buffer (pH 8.0). The purified chloroplast 2-Cys Prx exhibited a single band of 46 and 23 kDa in non-reducing and reducing SDS-PAGE, respectively (18). A molar extinction coefficient of 23,555 M^{-1} cm^{-1} at 280 nm was used to quantitate the homogeneous preparation of the recombinant protein. Recombinant chloroplast rapeseed Trx-m was prepared as reported previously (18).

Assay of Peroxidase and Chaperone Activities—The peroxidase activity was assayed at 25 °C as described previously (7). The chaperone activity of 2-Cys Prx was measured using bovine pancreas insulin as substrate. To this end, 2-Cys Prx (8–18 μM) was incubated at 25 °C in 20 mM Tris-HCl buffer (pH 8) containing 0.5 mg/ml insulin. After 5 min, dithiothreitol was added (20 mM), and the aggregation of insulin β-chain was followed at 25 °C by monitoring optical density at 600 nm.

8-Anilinonaphthalene-1-sulfonic Acid (ANS) Fluorescence—Fluorescence studies with ANS were performed at 25 °C in solutions of 20 mM Tris-HCl buffer (pH 8) containing 10 μM 2-Cys Prx, 75 μM ANS ($\epsilon_{350\,nm}$ = 5,000 M^{-1} cm^{-1}), 2 mM $MgCl_2$, and appropriate concentrations of ATP (0–5 mM). After 10 min, the samples were excited at 370 nm, and emission spectra were scanned from 400 to 600 nm (bandwidth 5 nm). Reported spectra were averaged over four scans taken at 90° relative to the direction of the incident beam. All measurements were corrected for both buffer and non-bound ANS. The spectral center of mass, *CM*, was calculated using the following equation,

$$CM = \frac{\sum_{i=1}^{N} mi}{\sum_{i=1}^{N} \frac{mi}{yi}} \qquad \text{(Eq. 1)}$$

where *mi* is the emission intensity at the *yi* wavelength and *N* is the spectrum range (23).

Dynamic Light Scattering (DLS)—Solutions of 20 mM Tris-HCl buffer (pH 8) containing 5 μM 2-Cys Prx were centrifuged at 14,000 rpm for 30 min. Insoluble debris was removed, and $MgCl_2$ (3 mM) containing appropriate concentrations of ATP (0–5 mM) were added to the supernatant fraction. DLS measurements were performed at 25 ± 0.1 °C using non-invasive back scatter equipment (Malvern Nano S, Malvern, UK) with a constant 173° scattering angle (sample volume 0.5 ml). A total of 25 scans (10 repetitions each) with an individual duration of ~2.4 min were obtained for each sample. Scattering intensities

were analyzed using the instrument software for the calculation of hydrodynamic diameter (D_H), size, and volume distribution.

Static Light Scattering (SLS)—The measurement of the molecular mass of 2-Cys Prx was carried out at 25 °C on a Precision Detector PD2010 light-scattering instrument connected in tandem to a Sephadex G-50 column and an LKB 2142 differential refractometer. 2-Cys Prx (43 μM) was incubated for 5 min in 50 mM Tris-HCl buffer (pH 7.8) in the presence and in the absence of 3 mM ATP and 3 mM $MgCl_2$. The protein was loaded on the Sephadex G-50 column equilibrated with the incubation solution and eluted with the same solution. The 90° light scattering and refractive index signals of the eluting material were analyzed with the Discovery32 software supplied by the manufacturer. Molecular masses were determined from the values of light scattering and refractive index using the model of Rayleigh-Debye-Gans for dilute polymer solutions.

Aggregation of 2-Cys Prx—2-Cys Prx (1–15 μM) was incubated at 25 °C for 10 min in 0.4 ml of 20 mM Tris-HCl buffer (pH 8) containing appropriate perturbants. The aggregation of the protein was started by the addition of both ATP and $MgCl_2$ and followed by monitoring the optical density at 600 nm in a Hitachi 220A dual beam spectrophotometer or by analysis of the supernatant and precipitate fractions on non-reducing SDS-PAGE.

Analysis of 2-Cys Prx Aggregation with Surface Plasmon Resonance (SPR)—The aggregation of 2-Cys Prx mediated by ATP/Mg was carried out on an IAsys instrument (NeoSensors Ltd., Durham, UK), using standard carboxymethyl-dextran chips where neither 2-Cys Prx nor ATP was covalently attached to the surface of the cuvette. For base-line stabilization, the cuvette was washed several times with 20 mM Tris-HCl buffer (pH 8) until the resonant angle response was constant. The instrument parameters were set at 100% for stirring and 0.3 s for the sampling interval, and all measurements were performed at 25 °C. To estimate the association parameters, 4.2 μM 2-Cys Prx, 3 mM $MgCl_2$, and appropriate concentrations of ATP were sequentially added. After every analysis, the cuvette surface was regenerated by washing three times with 4 M KOH (100 μl each) followed by several times with 20 mM Tris-HCl buffer (pH 8). The apparent association (k_a), dissociation (k_d), and equilibrium ($K_D = k_d/k_a$) constants were obtained from the linear regression plot ($k_{on} = k_a \times [ATP] - k_d$) using the FAST plot program. Alternatively, k_d was estimated by adding 10 mM EDTA to the cuvette after the association signal remained constant.

Transmission Electron Microscopy (TEM)—2-Cys Prx (0.1 mg/ml) was incubated at 25 °C in 20 mM Tris-HCl buffer (pH 8) and 3 mM $MgCl_2$, in the presence or in the absence of 3 mM ATP. After 5 min, an aliquot (20 μl) was disseminated onto a carbon-coated copper grid (mesh 300, Ted Pella, Redding, CA), the excess of solution was gently removed using filter paper, and the grid was air-dried for 1 min. The protein was negatively stained with 0.5% uranyl acetate (pH 4.5) for 1 min. The grid was air-dried, and samples were examined under a transmission electron microscope (Philips EM 301). Particle dimensions were estimated using ImageJ. At least three independent experiments were performed for each treatment of 2-Cys Prx.

Photochemical Cross-link of ATP with 2-Cys Prx—UV-mediated binding of ATP to 2-Cys Prx was carried out as described previously (24). Briefly, the protein (10 μM) in 20 mM Tris-HCl buffer (pH 8) containing 5 mM $MgC1_2$ and appropriate concentrations of ATP was irradiated at 25 °C with a 15-watt germicidal lamp (total volume 0.2 ml). After 35 min, the solution was dialyzed overnight at 4 °C against 20 mM sodium phosphate buffer (pH 8).

Circular Dichroism (CD)—CD spectra of 2-Cys Prx (2 μM) in 20 mM sodium phosphate buffer (pH 8) were measured at 20 °C with a quartz microcuvette (light path 0.2 cm) placed in a J-810 spectropolarimeter equipped with a thermoelectric temperature controller (Jasco, Easton, MD). Spectra were collected at 0.5 nm resolution and a scan rate of 200 nm/min, using at least two different preparations of freshly prepared protein solutions. Reported spectra were averaged over four scans. Ellipticities of CD spectra were analyzed with the software package CDPro, and the outputs of SELCON3, CONTINLL, and CDSSTR programs were averaged to quantitate the percentage of secondary structure of each spectrum.

RESULTS

Binding of ANS to 2-Cys Prx—ANS is a fluorescent probe that interacts with solvent-accessible non-polar regions of partially folded proteins, which would be relatively rare in the native state (25, 26). ANS binds to chloroplast 2-Cys Prx, causing a marked blue shift in the emission maximum wavelength (512 nm → 497 nm) and concurrently increasing the intensity of the fluorophore (7). Fig. 1*A* illustrates that the emission spectra of ANS exhibited modifications of the center of mass and intensity upon the incorporation of ATP in the presence of 2 mM Mg^{2+}. As illustrated in Fig. 1*B*, the response of the center of mass to increasing concentrations of ATP showed three well defined stages: (i) a significant blue shift (497 nm → 492 nm) at concentrations lower than 0.5 mM, (ii) a stabilization at 492 nm from 0.5 to 2 mM, and (iii) a second blue shift (492 nm → 489 nm) between 2 and 5 mM. Notably, these transitions of fluorescence emulated the ATP/Mg-mediated inhibition of the peroxidase activity reported previously (*cf.* Fig. 1 in Ref. 7). Taken together, the ATP-induced transitions appear to be related to changes in the tertiary structure and/or the self-association of 2-Cys Prx, which, in turn, drag the protein to populate states with more exposed hydrophobic regions. The interaction with ATP/Mg did not imply changes in the chemical state of the nucleotide because we found that neither ADP nor phosphate is incorporated to the protein or released to the surrounding milieu.

ATP/Mg Drive the Quaternary Structure of 2-Cys Prx to Larger Assemblies—The weight average molar mass of native 2-Cys Prx was 230 kDa in SLS experiments but the major species corresponded to a weight average molar mass of 46 kDa when estimated by gel filtration or non-reducing SDS-PAGE. In line with previous studies, these results confirmed that covalently linked homodimers of 2-Cys Prx have a tendency to associate non-covalently into decamers (27–29). Moreover, SLS experiments showed that the weight average molar mass of 2-Cys Prx increased from 230 kDa to 2.2 MDa upon the addition of 3 mM ATP/Mg, but it returned immediately to the former value when ATP was removed by gel filtration (not shown).

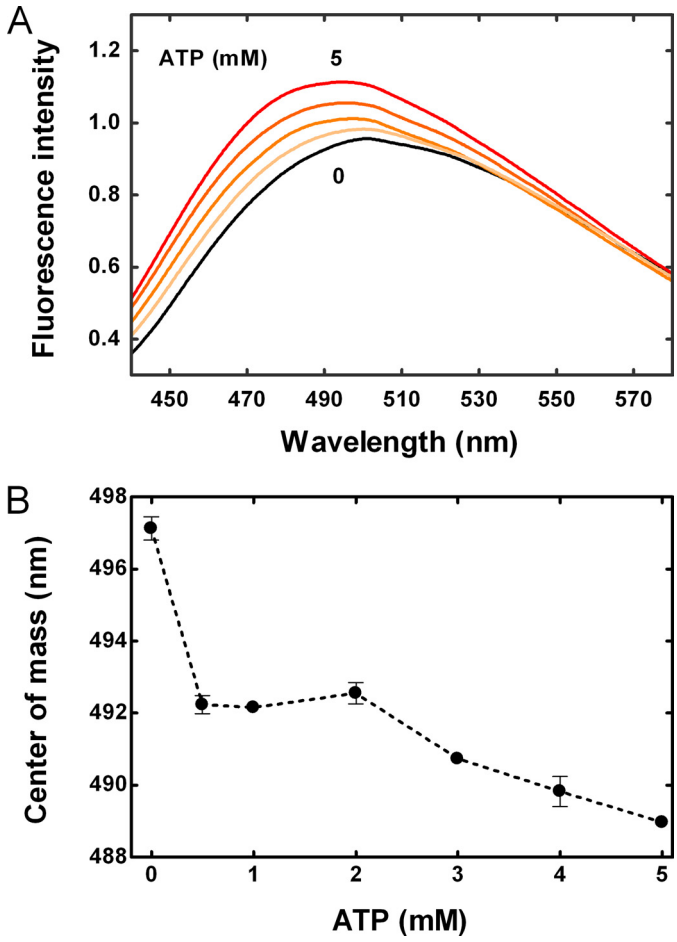

FIGURE 1. **Effect of ATP/Mg on the binding of ANS to 2-Cys Prx.** *A*, typical fluorescence emission spectra. Titration of ATP binding to 10 μM 2-Cys Prx in the presence of 2 mM Mg^{2+}. Emission spectra of ANS were measured after excitation at 370 nm. Every spectrum represents the difference between the average of four scans and the spectrum of ANS acquired in absence of 2-Cys Prx. *B*, center of mass for ANS-2-Cys Prx complexes. Every value (center of mass ± S.D. (*error bars*)) is the average of three independent experiments illustrated in *A*.

Given the fast interconversion between 2-Cys Prx decamers and large oligomers, we turned to DLS for studying the self-polymerization in real time. In the presence of 3 mM Mg^{2+}, the particle size distribution of 2-Cys Prx showed a homogeneous population centered at a D_H of 13 nm that remained invariable during the assay (Fig. 2*A*). This size was in line with the values obtained from structures of 2-Cys Prx decamers from different organisms (15, 28). When 4 mM ATP was added, the peak maximum shifted slowly to different species that approached a maximum of 40 nm in 30 min (Fig. 2*B*). This irregular time-dependent size distribution revealed that ATP/Mg induced the emergence of new oligomeric species from the monodisperse population of decamers. Two complementary experiments further indicated that the ATP/Mg-mediated oligomerization was an important feature of typical 2-Cys Prx. First, the *E. coli* homolog AhpC exhibited similar variations in the profile of D_H upon the addition of 4 mM ATP/Mg (not shown). Second, ATP/Mg did not modify the D_H of chloroplast Trx-m (4.2 nm), a monomeric protein that, like typical 2-Cys Prx, exhibits the Trx fold (supplemental Fig. S1) (30, 31). At this stage, we asked whether ATP/Mg drive 2-Cys Prx to the formation of irreversible or reversible oligomers in solution. The former process is often associated with modifications that denature proteins, whereas the latter is ascribed to self-associations that generally contribute to regulatory functions. The almost instantaneous dissociation of the large oligomers to initial decamers by the addition of EDTA demonstrated the reversibility of the process (Fig. 2*C*). Although we were able to trap oligomers that accumulate in solution when 2-Cys Prx was incubated with low concentrations of ATP, large supramolecular assemblies appeared beyond 4 mM (Fig. 2*D*). These novel species originated from the decameric form were far larger than most previous reports of soluble 2-Cys Prx oligomers (Fig. 2*E* is the enlarged *boxed section* of Fig. 2*D*).

Morphologic Analysis of 2-Cys Prx Assemblies—DLS experiments do not convey information on the shapes of particles. Therefore, TEM analyses were performed to assess the dependence of protein morphology on the binding of ATP/Mg. In the absence of ligands, proteins appear as ring-shaped structures with an average external diameter of 13 nm and an internal diameter of 6 nm (Fig. 3*A*), consistent with the decameric toroids observed in counterparts from other species (9, 32, 33). In contrast to these regular morphologies, treatment with 3 mM ATP/Mg (Fig. 3*B*) produced large ball-like particles with an average diameter of ~30 nm. Most of the spheres exhibited irregular surfaces that contained small discernible substructures, suggesting a residual heterogeneity within each class. Overall, TEM corroborated that the binding of ATP/Mg triggered the formation of oligomers whose quaternary structures were markedly different from the ring-shaped forms observed in the absence of ATP.

Secondary Structure of 2-Cys Prx·ATP/Mg Complexes—To further unravel the structural changes that promote the modification of the quaternary structure, we relied on far-UV CD spectroscopy to study the action of ligands on the elements of secondary structure. Although the approach was conceptually straightforward, the high extinction coefficient of ATP in the far-UV region precluded the direct use of CD spectroscopy due to a high noise/signal ratio. If the non-covalent binding of ATP to 2-Cys Prx has an effect upon the structure, the immobilization of the nucleotide through covalent binding should mimic the conformational change. We therefore used the method of photoaffinity labeling, which enabled the covalent binding of the nucleotide to regions of the protein in close contact with the adenine ring (34). The exposure of 2-Cys Prx to UV light in the presence of both [8-^{14}C]ATP and Mg^{2+} and subsequent analysis of the products by SDS-PAGE provided direct evidence for the formation of the photoadduct (supplemental Fig. S2, *A* and *B*). Next, we examined whether far-UV CD spectra of 2-Cys Prx were affected by the concentration of ATP during photolabeling. To this end, 2-Cys Prx was (i) incubated with 5 mM $MgCl_2$ and varying concentrations of ATP, (ii) exposed to UV light, and (iii) separated from the unbound nucleotide by dialysis (Fig. 4*A*). Fig. 4*B* shows that increasing concentrations of ATP during the photochemical reaction brought about two important changes in CD spectra: (i) a considerable decrease in the large positive ellipticity at 192 nm and (ii) a pronounced shift of negative minima at 222 and 208 nm to a unique minimum at 219 nm with a concurrent increase

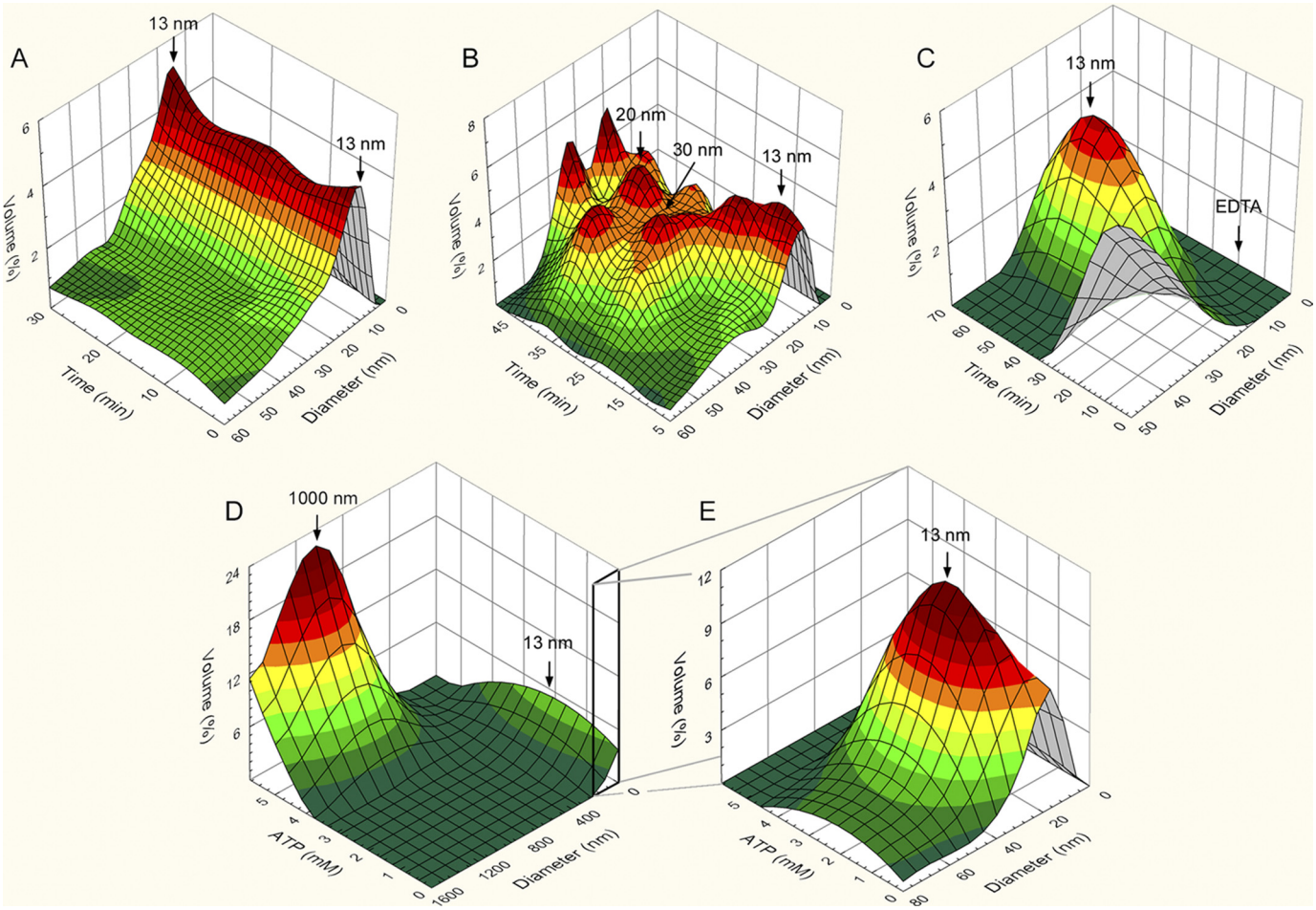

FIGURE 2. **Effect of ATP/Mg on the D_H of 2-Cys Prx.** 2-Cys Prx (5 μM) in 20 mM Tris-HCl buffer (pH 8) containing 3 mM $MgCl_2$ was incubated at 25 °C in the presence of 0 mM (*A*) and 3 mM (*B*) ATP. After 20 min, analyses by DLS were carried out as described under "Experimental Procedures." *C*, DLS analysis was performed after the incubation of 2-Cys Prx in the presence of 5 mM ATP followed by the addition of 10 mM EDTA. *D*, DLS of 2-Cys Prx after incubation with varying concentrations of ATP for 30 min. *E*, expanded view of plot *D* in the size range between 0 and 80 nm.

of ellipticity. The lack of an absolute convergence of the spectra onto an isodichroic point suggested that a simple two-state process did not account for changes in the secondary structure of 2-Cys Prx (35, 36). Analysis of the data showed that the proportion of α-helical structures fell from 33.2 to 10.0% and β-strands increased from 17.6 to 38.8%, whereas unordered and β-turn structures remained practically unchanged (Fig. 4*B*, *inset*). Taken together, data presented here are the first evidence of a physiological modulator, ATP, that interacts with 2-Cys Prx, inducing α-helix $\rightarrow$ β-sheet transitions, which, in turn, may lead to the self-polymerization of the protein.

Higher Concentrations of ATP/Mg Cause the Reversible Aggregation of 2-Cys Prx—Investigating the relationship between the quaternary structure of 2-Cys Prx and ATP/Mg binding, we unexpectedly found that 2-Cys Prx no longer remained soluble at concentrations of ATP over 5 mM. The presence of 5 mM ATP/Mg caused the immediate increase of light scattering to values proportional to 2-Cys Prx concentrations from 1 to 15 μM (Fig. 5*A*). Interestingly, no significant lag time preceded the formation of insoluble 2-Cys Prx that was completed in about 100 s. When the ligands were added separately, the insolubilization of 2-Cys Prx started upon the addition of the second ligand, indicating that the aggregation process was dependent on the simultaneous presence of both ATP and Mg^{2+} (supplemental Fig. S3*A*). Although ADP partially replaced ATP in this capacity, neither other nucleotides nor phosphate were functional (supplemental Fig. S3*B*). On the contrary, Mn^{2+}, Ca^{2+}, and Zn^{2+} were as efficient as Mg^{2+} in assisting ATP for the insolubilization of 2-Cys Prx (not shown).

We confirmed by SDS-PAGE the appearance of insoluble aggregates when the protein was incubated in solutions containing 5 mM ATP/Mg (Fig. 5*B*). Strikingly, these precipitates completely redissolved by adding EDTA (5 mM) or by dilution with 25 mM Tris-HCl buffer (pH 8) containing 5 mM $MgCl_2$. In line with a specific link between ATP/Mg and the structure of 2-Cys Prx, other chloroplast proteins (Trx-m and fructose-1,6-bisphosphatase) did not aggregate in the presence of ATP/Mg (supplemental Fig. S4) (18). It is evident from these results that the transition of 2-Cys Prx from soluble oligomers to insoluble aggregates is specifically induced by high concentrations of ATP/Mg ($\geq$5 mM) and completely reversed by removal of either ligand.

The ATP/Mg-mediated Aggregation of 2-Cys Prx Is Prevented by the Induction of Non-native Helical Conformations—If the ATP/Mg-mediated insolubilization of 2-Cys Prx was depen-

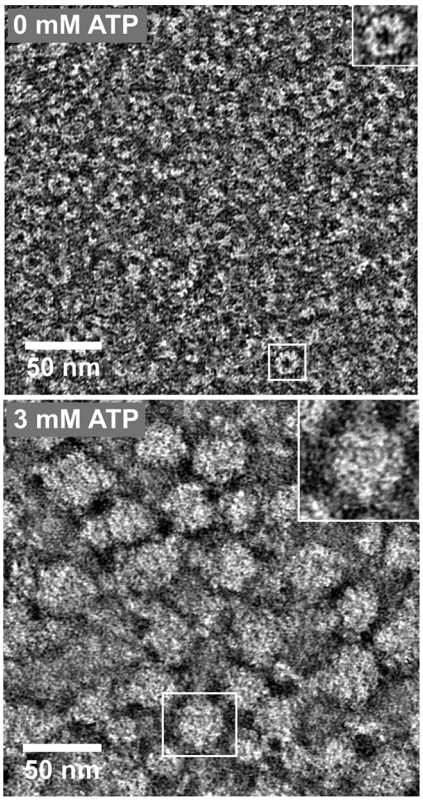

FIGURE 3. **TEM of 2-Cys Prx oligomers.** 2-Cys Prx (4.2 μM) was incubated at 25 °C in 20 mM Tris-HCl buffer (pH 8) and 3 mM $MgCl_2$ in the absence and in the presence of 3 mM ATP. The protein was stained with 0.5% (w/v) uranyl acetate and visualized by electron microscopy. *Scale bar*, 50 nm. *Insets*, *enlarged pictures* of representative particles (*framed*).

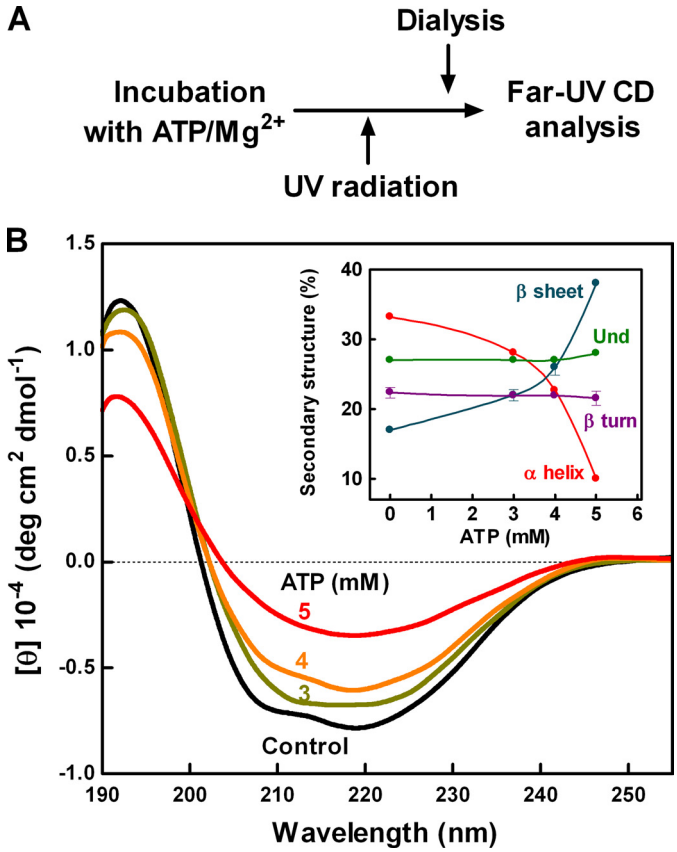

FIGURE 4. **Secondary structure of 2-Cys Prx·ATP complexes.** *A*, experimental outline. 2-Cys Prx (10 μM) dissolved in 0.1 ml of 20 mM Tris-HCl buffer (pH 8) and 5 mM $MgCl_2$ containing ATP, as indicated, was irradiated at 25 °C with an UV lamp. After 30 min, the solution was dialyzed overnight against 20 mM sodium phosphate buffer (pH 8). *B*, far-UV CD spectra. *Inset*, the content of secondary structure elements was estimated with the CDPro package software.

dent on the transition α-helix $\rightarrow$ β-sheet, the enhancement of more stable α-helix forms should favor the solubility of the protein. We thus explored initially the secondary structure of 2-Cys Prx by far-UV CD upon the addition of 2,2,2-trifluoroethanol (TFE), a cosolvent commonly used to induce α-helical conformations (37, 38). Both the small positive maximum at 192 nm and the negative minima at 208 and 222 nm indicated the presence of α-helices in the native protein (Fig. 6*A*). Increasing concentrations of TFE, however, enhanced the dichroic signals with a dramatic increment of the α-helical content (12.1% $\rightarrow$ 37.1%) at the expense of β-sheet structures (35.2% $\rightarrow$ 17.2%) beyond 5% (v/v) TFE (Fig. 6*A*, *inset*). Subsequently, we investigated the aggregation of 2-Cys Prx by light scattering when ATP/Mg were added into solutions containing different concentrations of TFE. As predicted, concentrations of TFE beyond 5% (v/v) inhibited the aggregation of 2-Cys Prx (Fig. 6*B*). These data were in line with the view that ATP/Mg promoted the formation of β-sheet structures and, in so doing, predisposed 2-Cys Prx to the relatively fast and reversible process of oligomerization and subsequent aggregation.

SPR Analysis of ATP/Mg-mediated Aggregation of 2-Cys Prx—We next implemented a new application of SPR to assess the kinetics of 2-Cys Prx aggregation. Monitoring the association of interacting molecules through SPR relies upon variations of the refractive index close to the sensor surface when soluble ligands bind to the partner molecule immobilized on SPR chips (39, 40). Because the resonant condition is extremely sensitive to the refractive index of the medium adjacent to the metal film, adsorption of large polypeptides or conformational changes of the attached proteins can be accurately detected (41, 42). On this basis, we reasoned that the formation of large aggregates on the surface of unmodified chips should also provide an optical measurement of ligand-mediated protein precipitations, both reactants being soluble notwithstanding. As predicted, the technique of SPR was effective for estimating the reversible aggregation of 2-Cys Prx caused by ATP/Mg (Fig. 7*A*). The sensorgram exhibited slight increases upon the addition of 5 mM Mg^{2+} but rose significantly after the incorporation of 6 mM ATP, resulting in a nearly 7-fold increase of SPR angle shift. The removal of Mg^{2+} by the addition of 10 mM EDTA diminished the SPR response. The dynamic data collected by the SPR sensor were further employed for the estimation of kinetic binding parameters. Using the linear regression of the pseudo-first-order rate constant ($k_{on} = k_a$. [ATP] $- k_d$) *versus* the respective concentration of ATP, we derived the apparent association ($k_a = 0.94 \pm 0.05$ M^{-1} s^{-1}) and dissociation ($k_d = (2.3 \pm 0.4) \times 10^{-3}$ s^{-1}) rate constants for the reversible aggregation of 2-Cys Prx (Fig. 7*B*). The apparent equilibrium dissociation constant (K_D) was calculated as $K_D = k_d/k_a$. Notably, this K_D (2.4 $\pm$ 0.1 mM) approached the previous second constant of ATP-mediated inhibition of the peroxidase activity

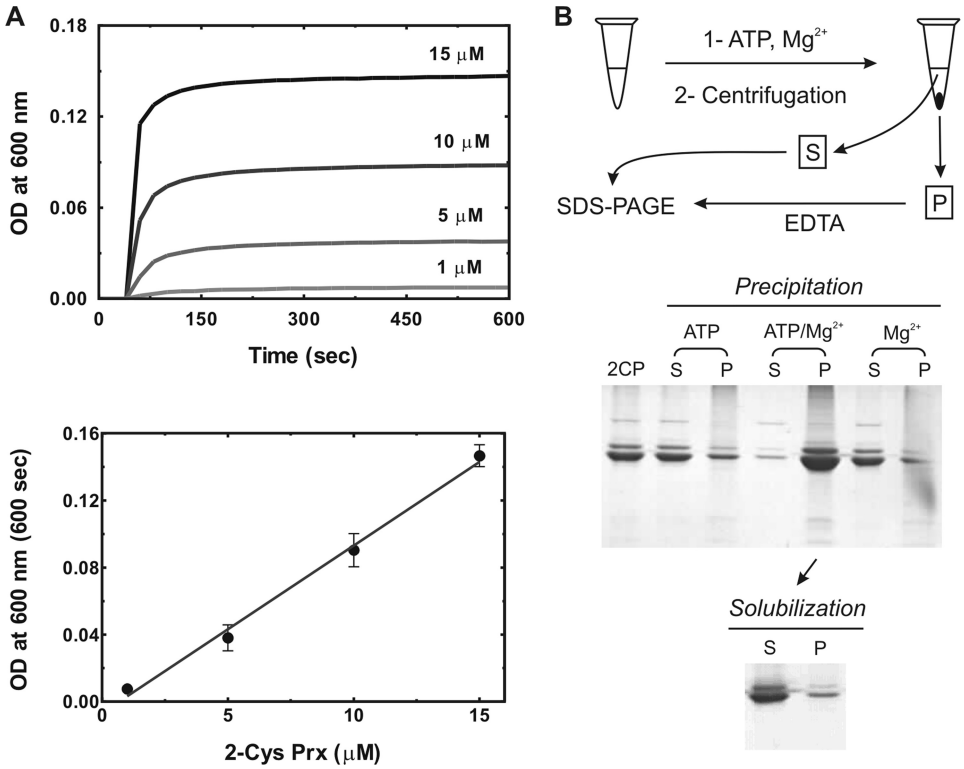

FIGURE 5. **Aggregation of 2-Cys Prx at high ATP/Mg concentrations.** *A*, kinetics of 2-Cys Prx precipitation. 2-Cys Prx (1–15 μM) dissolved in 20 mM Tris-HCl buffer (pH 8) was incubated at 25 °C. After the simultaneous addition of 5 mM ATP and 5 mM $MgCl_2$, the optical density was recorded at 600 nm. *Top*, typical time courses. *Bottom*, dependence of aggregation on the concentration of 2-Cys Prx. Each value represents the average ($OD_{660\ nm}$ ± S.D. (*error bars*)) of three independent experiments illustrated in the *top*. *B*, reversibility of the aggregation. *Precipitation*, 2-Cys Prx (10 μM) was incubated in the presence of 5 mM ATP and 5 mM $MgCl_2$, as indicated. After 10 min, the suspension was centrifuged, and the supernatant (*S*) and precipitate (*P*) fractions were subjected to non-reducing SDS-PAGE, using recombinant 2-Cys Prx as control (*lane 1*). *Resolubilization*, the precipitate of 2-Cys Prx was resuspended in 5 mM EDTA, centrifuged for 10 min, and subjected to non-reducing SDS-PAGE.

($I_{0.5}$ = 1.4 mM) (7). In summary, the dynamic monitoring of 2-Cys Prx aggregation by the novel use of SPR sensors not only facilitated the estimation of association and dissociation rates but also avoided interference frequently associated with spectrophotometry or fluorescence techniques, such as absorbance and quenching. However, our approach was not suitable to envision conformational changes, as previously suggested for dihydrofolate reductase (41) and transglutaminase (42), because 2-Cys Prx was not bound to the sensor surface.

Site-directed Mutants Reveal the Structural Independence of 2-Cys Prx Functions—The results described here provided the first evidence that two physiological ligands devoid of redox activity, ATP and Mg^{2+}, promote the self-polymerization of 2-Cys Prx, an additional feature to the specific regulation of peroxidase and chaperone activities (7). Earlier studies have revealed the necessary participation of two conserved arginines, Arg^{129} and Arg^{152}, in the peroxidase activity, but detailed information on the chaperone activity and the ATP/Mg-dependent oligomerization/aggregation was missing (43–47). Therefore, we set out to find whether mutants whose positively charged residues were replaced by the neutral alanine were functional in the latter functions. As expected, the substitution of Arg^{129} and Arg^{152} by alanine abrogated the ability of the active site to reduce H_2O_2 (Fig. 8). We next assayed the capacity of 2-Cys Prx variants to prevent the insolubilization of the β-chain upon the reductive cleavage of insulin. Surprisingly, this activity was greatly enhanced and almost abolished when the alanine residue replaced Arg^{129} and Arg^{152}, respectively. These contrasting effects unexpectedly revealed that the chaperone activity of 2-Cys Prx was not only independent of a functional peroxidatic site but also highly dependent on the position of amino acid residues crucial for the redox activity. When we next compared the responses of the wild type and mutant forms to ATP/Mg, the positively charged residues also appeared as important for the stabilization of the aggregates. However, at variance with the peroxidase and chaperone activities, the substitution of Arg^{129} reduced the propensity of 2-Cys Prx to aggregate in the presence of ATP/Mg, whereas the variant at Arg^{152} was mostly equivalent to the wild type form. Interestingly, neither the mutants nor the wild type counterpart exhibited an appreciable lag phase upon the addition of ATP/Mg. Overall, the site-directed mutagenesis of Arg^{129} and Arg^{152} confirmed earlier work concerning the peroxidase activity but revealed that the manifold functions of 2-Cys Prx are not strictly linked and, thus, can be uncoupled.

DISCUSSION

A large number of studies have demonstrated that the oxidation state of peroxidatic cysteine Cys_P governs the quaternary structure of typical 2-Cys Prxs (1, 28, 48). However, protein self-polymerization is not coupled exclusively to redox transformations of cysteine residues because the composition of the surrounding solvent and post-translational modifications also condition the proportion of 2-Cys Prx allocated to different

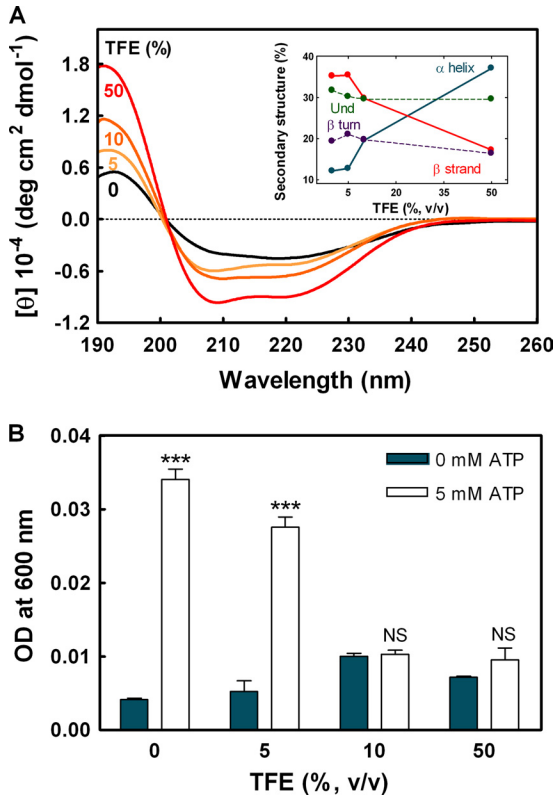

FIGURE 6. **Effect of TFE on ATP/Mg-mediated aggregation of 2-Cys Prx.** 2-Cys Prx (5 μM) was incubated at 25 °C in 0.4 ml of 20 mM sodium phosphate buffer (pH 8) containing 5 mM $MgCl_2$ and TFE, as indicated. *A*, far-UV CD spectra. *Inset*, the percentage of secondary structure was estimated with the CDPro package software. *B*, aggregation. 2-Cys Prx aggregation was started by the addition of 5 mM ATP, and, after 10 min, the optical density at 600 nm was recorded. The average value ($A_{660\ nm}$ ± S.D. (*error bars*)) of three independent experiments is plotted. The means with and without ATP were compared by Student's two-tailed *t* test for each TFE concentration used. ***, $p <$ 0.0001; *NS*, not significant.

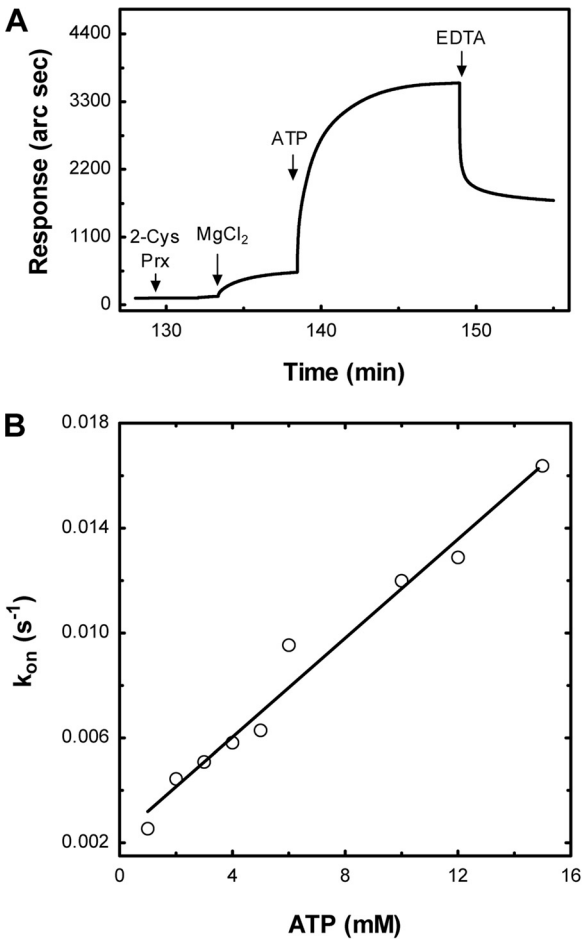

FIGURE 7. **SPR analysis of the 2-Cys Prx aggregation.** SPR was carried out on an IAsys instrument, as described under "Experimental Procedures." *A*, typical sensorgram. 2-Cys Prx (4.2 μM), $MgCl_2$ (5 mM), ATP (6 mM), and EDTA (10 mM) were added to the cuvette, as indicated. *B*, estimation of kinetic parameters of the ATP/Mg-induced aggregation of 2-Cys Prx. On-rates (k_{on}) were obtained by adding successively $MgCl_2$ and varying concentrations of ATP to 2-Cys Prx. The apparent kinetic constants were estimated from the linear regression plot of k_{on} *versus* [ATP], as described under "Experimental Procedures."

oligomers (11, 28, 44, 49–51). In line with this view, we found that the concerted action of two naturally occurring metabolites, ATP and Mg^{2+}, causes the reversible assembly of 2-Cys Prx into large soluble oligomers that coalesce as insoluble aggregates at higher concentrations of the nucleotide-cation complex. The absence of reductants and oxidants throughout the entire study excludes any redox mechanisms, ensuring unambiguously the regulation of self-polymerization through non-redox chemistry. Extending this study, we demonstrate that the dynamic modulation of 2-Cys Prx is specific for the nucleotide because the replacement of ATP with other phosphoryl-bearing compounds does not lead to the oligomerization/aggregation. Moreover, two disparate results sustain the view that structural constraints within the protein also have a major role in the ability to assemble reversibly into oligomeric structures. First, proteins holding the Trx fold characteristic of 2-Cys Prx (*e.g.* chloroplast Trx-m (3)) are insensitive to ATP/Mg. Second, the response of site-directed mutants is highly sensitive to the location of the substituted residue.

Data from size exclusion chromatography, SLS, DLS, and SPR allowed us to demonstrate that ATP/Mg-mediated modulation of the quaternary structure involves the reversible interconversion of three predominant species. 2-Cys Prx exists mainly as monodisperse decamers ($(\alpha_2)_5$; 223 kDa) that shift

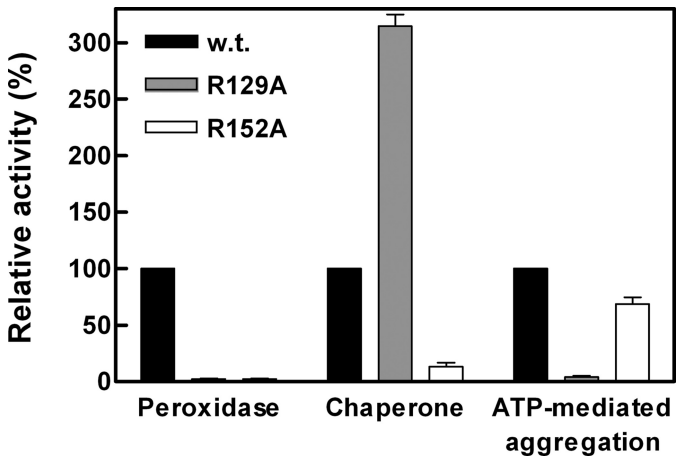

FIGURE 8. **Role of Arg^{129} and Arg^{159} in the functions of chloroplast 2-Cys Prx.** The peroxidase and chaperone activities and the ATP/Mg-mediated aggregation were assayed as described under "Experimental Procedures." Each function was assayed three times, and the average values of the variants were normalized to that of the wild type counterpart. *w.t.*, wild type; *error bars*, S.D.

toward polydisperse higher order oligomers ($(\alpha_2)_n > 2.3$ MDa ($n > 50$)) by increasing the concentrations of ATP. At higher concentrations of this nucleotide (≥5 mM), the product of oligomerization no longer remains in solution, building up a suspension of finely divided aggregates. TEM studies confirm the surprising versatility of 2-Cys Prx architectures. Consistent with observations of 2-Cys Prxs from other species (15), the chloroplast homolog assembles as toroidal decamers (external diameter 13 nm) in the absence of protein ligands but turns to larger round-shaped particles (external diameter ~30 nm) upon treatment with low concentrations of ATP/Mg. This assembly of chloroplast 2-Cys Prx into ball-like structures is reminiscent of, but different from, the erythrocyte counterpart that forms regular dodecahedrons containing 12 decamers with an external diameter of ~20 nm upon incubation with ammonium molybdate and polyethylene glycol (13).

A variety of studies have reported that the formation of partially unfolded intermediates precedes the oligomerization/aggregation of many proteins (52). Accordingly, significant modifications of maximal wavelengths and intensities of the extrinsic probe ANS indicate clearly that ATP/Mg enhance the proportions of exposed hydrophobic regions in 2-Cys Prx (25, 53). Moreover, like other proteins (54, 55), complementary strategies indicate that the ordered self-polymerization of 2-Cys Prx *in vitro* is caused by subtle rearrangements of secondary structural elements that have a net impact on the tertiary structure of monomers. The binding of ATP/Mg to 2-Cys Prx enhances the content of β-sheet elements and decreases the proportion of α-helical structures, leading to the fast and reversible oligomerization/aggregation. Consistent with the transition α-helices $\rightarrow$ β-sheets, the aggregation of 2-Cys Prx is impaired by TFE, a cosolvent that promotes the formation of α-helical structures. One of the remarkable aspects of this finding is that similar rearrangements from the native forms to non-native β-sheet structures with a concomitant propensity to ordered aggregates have also been reported in other proteins, such as amyloids and prion proteins (56, 57). Further analyses, however, disclose that differences between the latter and 2-Cys Prx are not simply the shape and size of aggregates but also the kinetics of formation (*cf.* below).

The formation of soluble oligomers and insoluble aggregates is a complex mechanism due to the delicate balance in the interaction between polypeptides and the surrounding solution, a process that embraces the packing of proper side chains (58, 59). Akin to contributions of specific amino acid residues, we have found that the ATP/Mg-mediated self-polymerization of 2-Cys Prx is impaired by the replacement of Arg^{129} by alanine but is insensitive to similar substitution at Arg^{152}. When compared with the effects on the peroxidase and chaperone activities, it is evident that 2-Cys Prx performs autonomous and unrelated activities without partitioning into different domains of the protein. As expected (44, 47), the replacement of Arg^{129} and Arg^{152} by alanine strongly reduced the peroxidase activity, but unexpectedly, the former enhanced whereas the latter almost abrogated the chaperone activity. In consequence, these conserved arginines play important roles not only in the peroxidase activity but also in the chaperone activity and the ATP/Mg-mediated self-assembly of 2-Cys Prx, revealing that determinants responsible for these disparate functions overlap.

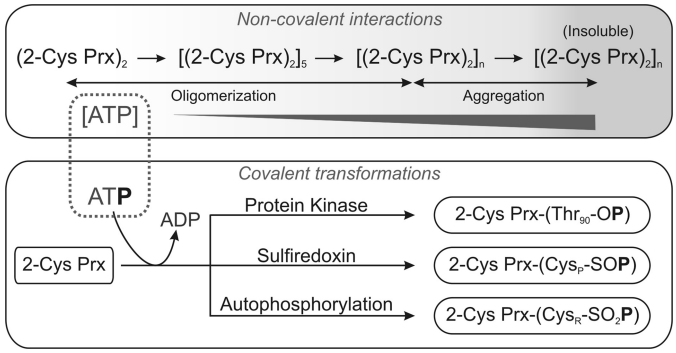

FIGURE 9. **The complex response of 2-Cys Prx to ATP/Mg.** Schematic representation of the roles that ATP plays in the regulation of 2-Cys Prx: as *ligand* for the modification of non-covalent interactions and as *substrate* for the covalent transformation of amino acid residues. ATP/Mg promotes the formation of soluble oligomers (oligomerization) that coalesce beyond critical concentrations of ligands into insoluble aggregates (aggregation). Cyclin-dependent *protein kinases* catalyze the incorporation of the phosphoryl moiety into specific threonine residues of 2-Cys Prx. In addition, ATP can phosphorylate both Cys_P and Cys_R, respectively. The *sulfiredoxin*-dependent conversion of sulfinic acid back to sulfenic acid implies the phosphorylation of Cys_P, although the sulfinic-phosphoryl anhydride was not isolated. In contrast to kinase- and sulfiredoxin-mediated phosphorylations, the *autophosphorylation* of Cys_R does not require an additional catalyst.

A myriad of non-covalent interactions between proteins and ligands have been identified in the aggregation of proteins associated with physiological and pathological processes. Naturally occurring self-polymerization of proteins can be grouped into two classes: *normal*, such as the reversible conversion *n*(G-actin) ⇔ *n*(F-actin), and *abnormal*, such as the irreversible transformation of *soluble oligomers* (α-synuclein) ⇒ *insoluble fibrils* (α-synuclein) in Parkinson disease (60). However, it is difficult to reconcile these processes with the reversible self-polymerization of 2-Cys Prx. Physiologically self-polymerizing proteins like actin and tubulin exploit the intrinsic free energy of nucleotide hydrolysis for rapid bursts of polymerization/depolymerization. In contrast, the elongation of amyloid fibrils is independent of nucleotide binding and attributed to the slow (>24 h) and irreversible assembly of a critical nucleus in the polymerization mechanism (61, 62). At variance, light-scattering data and our novel use of biosensors reveal the fast (<5 s) and reversible self-polymerization of 2-Cys Prx without any change in the chemical state of ATP. Hence, the latter equilibria may be exploited for carefully controlled purposes in cell metabolism because reversibility assists cellular components to circumvent the formation of kinetically trapped complexes on their way to the thermodynamically favored products.

The role of 2-Cys Prx in cell signaling has been associated primarily with oxidative stress, but the integration of signals from different pathways is as yet poorly understood (1, 63, 64). Present data show that, like redox transformations of the two conserved cysteine residues, metabolites indigenous to cells regulate the quaternary structure of 2-Cys Prx. Indeed, ATP plays a dual role in the structural regulation of 2-Cys Prx: substrate for the phosphorylation of specific residues (7, 11, 65–67) and modulator of the complex quaternary structures (7) (Fig. 9). The novelty of this allosteric modulation lies in the notion that the binding of ATP/Mg modifies the relative proportion of

secondary structures, thereby driving 2-Cys Prx to a dynamic exchange between three predominant species, two soluble and one insoluble: decamers ⇔ oligomers ⇔ amorphous aggregates. This interconversion of 2-Cys Prx quaternary structures evinces a number of features that are prototypical of metabolic signals coupled to environmental stimuli: (i) temporal regulation on physiological time scales, (ii) reversibility, (iii) protein motifs that facilitate ligand binding and provide specificity, and (iv) colocalization of the protein with a source of ligands sensitive to external stimuli. Of note, it is already known that not only do plant 2-Cys Prxs localize exclusively in the chloroplast stroma but also the levels of ATP and Mg^{2+} increase in this compartment when light triggers photosynthesis (14). In summary, we reveal unambiguously the ATP/Mg-dependent oligomerization of 2-Cys Prx, which may subserve signaling in cell physiology, coupling the status of cellular energy with redox processes at conserved cysteine residues. For such interactions to have physiological significance, the challenge now is to explore in more detail how responses of 2-Cys Prx to non-redox stimulus are coupled to those elicited via H_2O_2.

Acknowledgments—We thank Natalio De Vincenzo and Dr. Lia Pietrasanta (Centro de Microscopía Avanzada, Facultad de Ciencias Exactas y Naturales, Universidad de Buenos Aires) for help with TEM studies. We are grateful to Dr. Ana Cahuerff and Dr. Patricio Craig for assistance in DLS and SLS techniques.

REFERENCES

1. Hall, A., Karplus, P. A., and Poole, L. B. (2009) *FEBS J.* **276,** 2469–2477
2. Aran, M., Ferrero, D. S., Pagano, E., and Wolosiuk, R. A. (2009) *FEBS J.* **276,** 2478–2493
3. Copley, S. D., Novak, W. R., and Babbitt, P. C. (2004) *Biochemistry* **43,** 13981–13995
4. Hofmann, B., Hecht, H. J., and Flohé, L. (2002) *Biol. Chem.* **383,** 347–364
5. Noguera-Mazon, V., Krimm, I., Walker, O., and Lancelin, J. M. (2006) *Photosynth. Res.* **89,** 277–290
6. Soito, L., Williamson, C., Knutson, S. T., Fetrow, J. S., Poole, L. B., and Nelson, K. J. (2011) *Nucleic Acids Res.* **39** (Database issue), D332–D337
7. Aran, M., Caporaletti, D., Senn, A. M., Tellez de Iñon, M. T., Girotti, M. R., Llera, A. S., and Wolosiuk, R. A. (2008) *FEBS J.* **275,** 1450–1463
8. Chuang, M. H., Wu, M. S., Lo, W. L., Lin, J. T., Wong, C. H., and Chiou, S. H. (2006) *Proc. Natl. Acad. Sci. U.S.A.* **103,** 2552–2557
9. Jang, H. H., Lee, K. O., Chi, Y. H., Jung, B. G., Park, S. K., Park, J. H., Lee, J. R., Lee, S. S., Moon, J. C., Yun, J. W., Choi, Y. O., Kim, W. Y., Kang, J. S., Cheong, G. W., Yun, D. J., Rhee, S. G., Cho, M. J., and Lee, S. Y. (2004) *Cell* **117,** 625–635
10. Moon, J. C., Hah, Y. S., Kim, W. Y., Jung, B. G., Jang, H. H., Lee, J. R., Kim, S. Y., Lee, Y. M., Jeon, M. G., Kim, C. W., Cho, M. J., and Lee, S. Y. (2005) *J. Biol. Chem.* **280,** 28775–28784
11. Jang, H. H., Kim, S. Y., Park, S. K., Jeon, H. S., Lee, Y. M., Jung, J. H., Lee, S. Y., Chae, H. B., Jung, Y. J., Lee, K. O., Lim, C. O., Chung, W. S., Bahk, J. D., Yun, D. J., Cho, M. J., and Lee, S. Y. (2006) *FEBS Lett.* **580,** 351–355
12. Wood, Z. A., Schröder, E., Robin Harris, J., and Poole, L. B. (2003) *Trends Biochem. Sci.* **28,** 32–40
13. Meissner, U., Schröder, E., Scheffler, D., Martin, A. G., and Harris, J. R. (2007) *Micron* **38,** 29–39
14. König, J., Baier, M., Horling, F., Kahmann, U., Harris, G., Schürmann, P., and Dietz, K. J. (2002) *Proc. Natl. Acad. Sci. U.S.A.* **99,** 5738–5743
15. Schröder, E., Littlechild, J. A., Lebedev, A. A., Errington, N., Vagin, A. A., and Isupov, M. N. (2000) *Structure* **8,** 605–615
16. Cha, M. K., Yun, C. H., and Kim, I. H. (2000) *Biochemistry* **39,** 6944–6950
17. Phalen, T. J., Weirather, K., Deming, P. B., Anathy, V., Howe, A. K., van der Vliet, A., Jönsson, T. J., Poole, L. B., and Heintz, N. H. (2006) *J. Cell Biol.* **175,** 779–789
18. Caporaletti, D., D'Alessio, A. C., Rodriguez-Suarez, R. J., Senn, A. M., Duek, P. D., and Wolosiuk, R. A. (2007) *Biochem. Biophys. Res. Commun.* **355,** 722–727
19. Muthuramalingam, M., Seidel, T., Laxa, M., Nunes de Miranda, S. M., Gärtner, F., Ströher, E., Kandlbinder, A., and Dietz, K. J. (2009) *Mol. Plant* **2,** 1273–1288
20. Chen, C. Y., Willard, D., and Rudolph, J. (2009) *Biochemistry* **48,** 1399–1409
21. Kumsta, C., and Jakob, U. (2009) *Biochemistry* **48,** 4666–4676
22. Mora-Garcia, S., Stolowics, F., and Wolosiuk, R. A. (2005) in *Control of Primary Metabolism in Plants* (Plaxton, W., and McManus, M., eds) *Annu. Plant Rev.*, Vol. 22, pp. 150–186, Blackwell Publishing, Oxford, U.K.
23. Silva, J. L., Miles, E. W., and Weber, G. (1986) *Biochemistry* **25,** 5780–5786
24. Kaur, P., and Rosen, B. P. (1993) *J. Bacteriol.* **175,** 351–357
25. Semisotnov, G. V., Rodionova, N. A., Razgulyaev, O. I., Uversky, V. N., Gripas', A. F., and Gilmanshin, R. I. (1991) *Biopolymers* **31,** 119–128
26. Ptitsyn, O. B. (1995) *Adv. Protein Chem.* **47,** 83–229
27. Hirotsu, S., Abe, Y., Okada, K., Nagahara, N., Hori, H., Nishino, T., and Hakoshima, T. (1999) *Proc. Natl. Acad. Sci. U.S.A.* **96,** 12333–12338
28. Wood, Z. A., Poole, L. B., Hantgan, R. R., and Karplus, P. A. (2002) *Biochemistry* **41,** 5493–5504
29. Alphey, M. S., Bond, C. S., Tetaud, E., Fairlamb, A. H., and Hunter, W. N. (2000) *J. Mol. Biol.* **300,** 903–916
30. Duek, P. D., and Wolosiuk, R. A. (2001) *Biochim. Biophys. Acta* **1546,** 299–311
31. Atkinson, H. J., and Babbitt, P. C. (2009) *PLoS Comput. Biol.* **5,** e1000541
32. Sayed, A. A., and Williams, D. L. (2004) *J. Biol. Chem.* **279,** 26159–26166
33. Harris, J. R., Schröder, E., Isupov, M. N., Scheffler, D., Kristensen, P., Littlechild, J. A., Vagin, A. A., and Meissner, U. (2001) *Biochim. Biophys. Acta* **1547,** 221–234
34. Kierdaszuk, B., and Eriksson, S. (1988) *Biochemistry* **27,** 4952–4956
35. Chellgren, B. W., Miller, A. F., and Creamer, T. P. (2006) *J. Mol. Biol.* **361,** 362–371
36. Fändrich, M., Forge, V., Buder, K., Kittler, M., Dobson, C. M., and Diekmann, S. (2003) *Proc. Natl. Acad. Sci. U.S.A.* **100,** 15463–15468
37. Jayaraman, G., Kumar, T. K., Arunkumar, A. I., and Yu, C. (1996) *Biochem. Biophys. Res. Commun.* **222,** 33–37
38. Starzyk, A., Barber-Armstrong, W., Sridharan, M., and Decatur, S. M. (2005) *Biochemistry* **44,** 369–376
39. Schuck, P., Boyd, L. F., and Andersen, P. S. (1999) in *Curr. Protoc. Protein Sci.* (Coligan, J. E., Dunn, B. M., Speicher, D. W., and Wingfield, P. T., eds) Vol. 3, pp. 20.2.1–20.2.22, John Wiley & Sons, New York
40. Winzor, D. J. (2003) *Anal. Biochem.* **318,** 1–12
41. Sota, H., Hasegawa, Y., and Iwakura, M. (1998) *Anal. Chem.* **70,** 2019–2024
42. Gestwicki, J. E., Hsieh, H. V., and Pitner, J. B. (2001) *Anal. Chem.* **73,** 5732–5737
43. Montemartini, M., Kalisz, H. M., Hecht, H. J., Steinert, P., and Flohé, L. (1999) *Eur. J. Biochem.* **264,** 516–524
44. König, J., Lotte, K., Plessow, R., Brockhinke, A., Baier, M., and Dietz, K. J. (2003) *J. Biol. Chem.* **278,** 24409–24420
45. Poole, L. B. (2007) *Subcell. Biochem.* **44,** 61–81
46. Flohé, L., Budde, H., Bruns, K., Castro, H., Clos, J., Hofmann, B., Kansal-Kalavar, S., Krumme, D., Menge, U., Plank-Schumacher, K., Sztajer, H., Wissing, J., Wylegalla, C., and Hecht, H. J. (2002) *Arch. Biochem. Biophys.* **397,** 324–335
47. Nagy, P., Karton, A., Betz, A., Peskin, A. V., Pace, P., O'Reilly, R. J., Hampton, M. B., Radom, L., and Winterbourn, C. C. (Mar 8, 2011) *J. Biol. Chem.* 10.1074/jbc.M111.232355
48. Matsumura, T., Okamoto, K., Iwahara, S., Hori, H., Takahashi, Y., Nishino, T., and Abe, Y. (2008) *J. Biol. Chem.* **283,** 284–293
49. Chauhan, R., and Mande, S. C. (2001) *Biochem. J.* **354,** 209–215
50. Kitano, K., Niimura, Y., Nishiyama, Y., and Miki, K. (1999) *J. Biochem.* **126,** 313–319
51. Kristensen, P., Rasmussen, D. E., and Kristensen, B. I. (1999) *Biochem. Biophys. Res. Commun.* **262,** 127–131

52. Scheibel, T., and Serpell, L. (2005) in *Protein Folding Handbook* (Buchner, J., ed) pp. 197–253, Wiley-VCH, Weinheim, Germany
53. Stefani, M., and Dobson, C. M. (2003) *J. Mol. Med.* **81,** 678 – 699
54. Carulla, N., Zhou, M., Giralt, E., Robinson, C. V., and Dobson, C. M. (2010) *Acc. Chem. Res.* **43,** 1072–1079
55. Miller, Y., Ma, B., and Nussinov, R. (2010) *Chem. Rev.* **110,** 4820 – 4838
56. Pan, K. M., Baldwin, M., Nguyen, J., Gasset, M., Serban, A., Groth, D., Mehlhorn, I., Huang, Z., Fletterick, R. J., and Cohen, F. E. (1993) *Proc. Natl. Acad. Sci. U.S.A.* **90,** 10962–10966
57. Wetzel, R. (2006) *Acc. Chem. Res.* **39,** 671 – 679
58. Bemporad, F., Calloni, G., Campioni, S., Plakoutsi, G., Taddei, N., and Chiti, F. (2006) *Acc. Chem. Res.* **39,** 620 – 627
59. Goehring, A. S., Rivers, D. M., and Sprague, G. F., Jr. (2003) *Eukaryot. Cell* **2,** 930 –936
60. Morris, A. M., Watzky, M. A., and Finke, R. G. (2009) *Biochim. Biophys. Acta* **1794,** 375–397
61. Kueh, H. Y., and Mitchison, T. J. (2009) *Science* **325,** 960 –963
62. Chiti, F., and Dobson, C. M. (2006) *Annu. Rev. Biochem.* **75,** 333–366
63. Rhee, S. G., and Woo, H. A. (2011) *Antioxid. Redox Signal.*, doi: 10.1089/ars.2010.3393
64. Dietz, K. J., Jacquot, J. P., and Harris, G. (2010) *New Phytol.* **188,** 919 –938
65. Chang, T. S., Jeong, W., Choi, S. Y., Yu, S., Kang, S. W., and Rhee, S. G. (2002) *J. Biol. Chem.* **277,** 25370 –25376
66. Qu, D., Rashidian, J., Mount, M. P., Aleyasin, H., Parsanejad, M., Lira, A., Haque, E., Zhang, Y., Callaghan, S., Daigle, M., Rousseaux, M. W., Slack, R. S., Albert, P. R., Vincent, I., Woulfe, J. M., and Park, D. S. (2007) *Neuron* **55,** 37–52
67. Zykova, T. A., Zhu, F., Vakorina, T. I., Zhang, J., Higgins, L. A., Urusova, D. V., Bode, A. M., and Dong, Z. (2010) *J. Biol. Chem.* **285,** 29138 –29146